Modelling and simulation of a hybrid system of trickle bed reactor and multistage reverse osmosis process for the removal of phenol from wastewater

Jude S. Al-Huwaidi[1], Mudhar A. Al-Obaidi[2], Aysar T. Jarullah[3], Chakib Kara-Zaïtri[1] and Iqbal M. Mujtaba[1, *]

[1] Department of Chemical Engineering, Faculty of Engineering and Informatics. University of Bradford. Bradford, West Yorkshire, BD7 1DP, UK

[2] Middle Technical University, Technical Institute of Baquba, Dayala – Iraq

[3]Chemical Engineering Department, College of Engineering, Tikrit University, Iraq

***Corresponding author, Tel.: +44 0 1274 233645**

E-mail address: I.M.Mujtaba@bradford.ac.uk

Abstract

Phenol is one of the most toxic and harmful pollutants in industrial wastewater streams, the removal of which is therefore of critical importance. The use of reverse osmosis (RO) systems as a means of treating wastewater is continuously growing. This research investigates the effect of operating parameters on the performance of five different multistage RO configurations coupled with a trickle bed reactor (TBR) using model-based simulation. The results were compared, and an analysis was then performed to identify which hybrid TBR and multistage RO arrangement rejected the most phenol content. The basis for comparison was four performance metrics of permeate concentration, rejection, recovery, and specific energy. The study found that the flow rate and concentration have little effect on the operation unless there is a concurrent increase of both. It was also found that the four-performance metrics used were interlinked and affect the quality and quantity of the final freshwater product.

Keywords: Phenol Treatment; Trickled Bed Reactor; Multistage Reverse Osmosis; Modelling, Simulation.

1. Introduction

The availability of water in everyday human life is, to the greatest extent, profound. However, only 3% of the world's naturally occurring water sources are potable, where the remaining 97% of available water is saltwater (Spellman, 2020). The presence of a potable water source is often scarce or inaccessible in many parts of the world, such as countries with arid environments causing irregular or sparse rainfall periods (AlEisa et al., 2019). An increase of the global water demand would also increase the risk of water depletion (Duran-Llacer et al., 2020).

Whilst the amount of freshwater in the world today is finite, the amount of wastewater is significantly increasing year by year. Therefore, there is an urgent need for more innovative and efficient methods to treating wastewater.

Several petrochemical and pharmaceutical industries manufacture a great variety of products such as solvent, paint, dye, paper, pulp, and plastic, all of which yield large volumes of wastewater laced with phenolic by-products (Abdelkreem, 2013). These phenolic by-products and derivatives are extremely harmful, highly toxic, and life-threatening pollutants (EPA, 2002). This comes as a challenge, as industrial wastewater laced with phenolic by-products can sometimes be released into surface water, like rivers, lakes, and wetlands (Li, 2018). This is detrimental to the welfare of humans, and it is harmful to biodiversity and aquatic ecosystems. Phenol has been classed as one of the most toxic contaminants by the EPA and NPRI, to the extent of the WHO setting a 1 ppb limit of phenol in surface water (Gami et al., 2014; Villegas et al., 2016).

The many harmful effects of phenol thereby necessitate the treatment of wastewater to strip it of harmful pollutants before releasing it into the environment. Wastewater can be treated using several physical and chemical methods (Mohammadi et al., 2014). Traditional phenol removal methods consist of separation and destruction methods, which include distillation, adsorption, biodegradation, extraction, and chemical oxidation. However, more advanced phenol removal methods use oxidation processes, such as electrochemical, photo-oxidation, chemical oxidation; membrane technologies, and hybrid systems (Al-Obaidi et al., 2018a).

One of the most recent phenol removal method (Mnif et al., 2015) uses a polyamide thin film composite RO membrane called AG2514 TF manufactured by a company called Osmonics, where the phenol removal rate exceeds 40% and is even expected to reach 80%. Anku et al. (2016) studied the effectiveness of membrane technologies (RO) for the removal of phenolic compounds from wastewater. Mohammed et al. (2016) confirmed the efficiency of using a TBR with a catalytic wet air oxidation (CWAO) process to remove phenol. Al-Obaidi et al. (2017) used a spiral wound RO to remove phenol, and they corroborated their results with that available in literature. Their research confirmed that the spiral wound RO process is an effective method for removing phenol from wastewater.

Hybrid systems have gained a lot of attention recently, due to their effectivity and efficiency as wastewater treatment processes. They have proven to be superior to individual systems, where two or more treatment methods have been combined to enhance the effluent quality of wastewater (Tee et al., 2015). The RO system, although an outstanding method to treat impure water, do not usually act alone. There is usually an additional chemical or physical process, or a combination of both which makes for the best RO treatment outcome. These additional systems can be filtration, oxidation, or coagulation/flocculation sedimentation process prior to the RO process (Dupont et al., 1982). This is true for other treatment processes as well, in which an individual process may work well to some extent on its own, but does not deliver the excellence it may be able deliver if hybridized. Hybrid systems have also been proven to generate robust energy saving potentials (Tee et al., 2015). This has therefore provided an impetus for exploring hybrid systems further for the removal of phenol from wastewater.

The RO is widely known to be cost effective due to its low capital costs and energy saving characteristics (Akashah et al., 1987), while the TBR too has many cost effective qualities such as low catalyst damage which is attributed to cost savings, as well as low pressure drops which attributed to low pumping costs. The hybridization of these two technologies is predicted to generate favourable outcomes in terms of functionality, cost efficiency and energy saving. Al-Obaidi et al. (2018a) has

already combined a TBR with an RO system to achieve a more reliable method for removing phenol from industrial effluents. The aim of this research is to investigate the efficiency of a novel multistage RO and TBR hybrid system for the treatment of phenol in wastewater. To successfully conduct this research, five multistage RO process configurations are tested in a hybrid multistage RO and TBR system using gPROMS, including parallel, series, tapered and permeate reprocessing designs. Al-Obaidi et al. (2018a) developed a specific model to express the performance of a TBR and single RO membrane process. This model will be used as a basis to develop specific sets of sub-models to evaluate the performance of various hybrid RO and TBR system configurations. This paper uses the five hybrid systems to carry out a detailed simulation, based on a unique set of input parameters; where the results are then compared to the TBR and single membrane RO hybrid system of Al-Obaidi et al. (2018a). The net result of the comparison is used to identify the most effective hybrid system configuration which will yield the best permeate concentration and energy consumption.

2. Process Description

The two process options relevant to this research are Reserve Osmosis (RO) and Trickle Bed Reactor (TBR), and they described in greater detail in the following sections.

2.1 Reserve Osmosis (RO)

Reverse osmosis (RO) continues to offer a promising method for the separation of organic compounds from aqueous solutions in wastewater treatment processes, as highlighted by Huang et al. (2015). The RO process can be executed at ambient temperatures – meaning no boiler is required, the process has no phase changes, and less scaling and corrosion takes place. The reliability, availability, and economic efficiency of this process has been noted to be excellent, however, the top benefit is the low energy consumption that is associated with this process (Akashah et al., 1987). RO is able to have a long membrane life, low operating pressure, and reduced cleaning frequencies if quality pretreatment is practiced (Alhumoud et al., 2010). RO is a membrane-based process used to treat

wastewater containing organic compounds of low concentrations and low molecular weights (Villegas et al., 2016; Al-Obaidi et al., 2018d). The feed water is pushed through the pores of a semipermeable membrane under pressure, thus separating organic compounds from purified permeate water (Garud et al., 2011). In this process, the operating principles rely on the solvent's rate of transport through the semipermeable membrane, which is a function of pressure, area, membrane characteristics, and the solution temperature (Dupont et al., 1982).

2.2 Trickle Bed Reactor (TBR)

The catalytic wet air oxidation process (CWAO) is also often used in wastewater treatment industries for the oxidation of organic compounds in aqueous solutions. This oxidation process uses normal air or pure oxygen within a bed reactor packed with a solid catalyst. The bed reactor of choice here is a trickle bed reactor (TBR), under specified reactor operating conditions such as temperature and pressure, but also under other conditions such as the partial pressure of oxygen, gas flowrate, initial organic compound matter, and the hourly space velocity of wastewater. The TBR is a continuous packed bed reactor, which allows liquids to travel in a downward motion into the packing medium, causing a trickling effect (Wu et al., 2016). This process requires a coolant for the regulation of the heated outlet stream of the bed-reactor, as well as a separator for the separation of excess gas. A CWAO process in TBRs can remove 60% to 90% of phenol from industrial effluent streams, given certain operating conditions (Mujtaba et al., 2020).

2.3 The proposed process

In this research, the TBR and RO processes are integrated to form a hybrid TBR and multistage RO system, as shown in Fig. 1. To the best of knowledge of the authors, the idea of a combined TBR and multistage RO model has not been explored previously, although Al-Obaidi et al. (2018a) did consider a hybrid TBR and RO but a with a single membrane module of an area of 0.75 m^2.

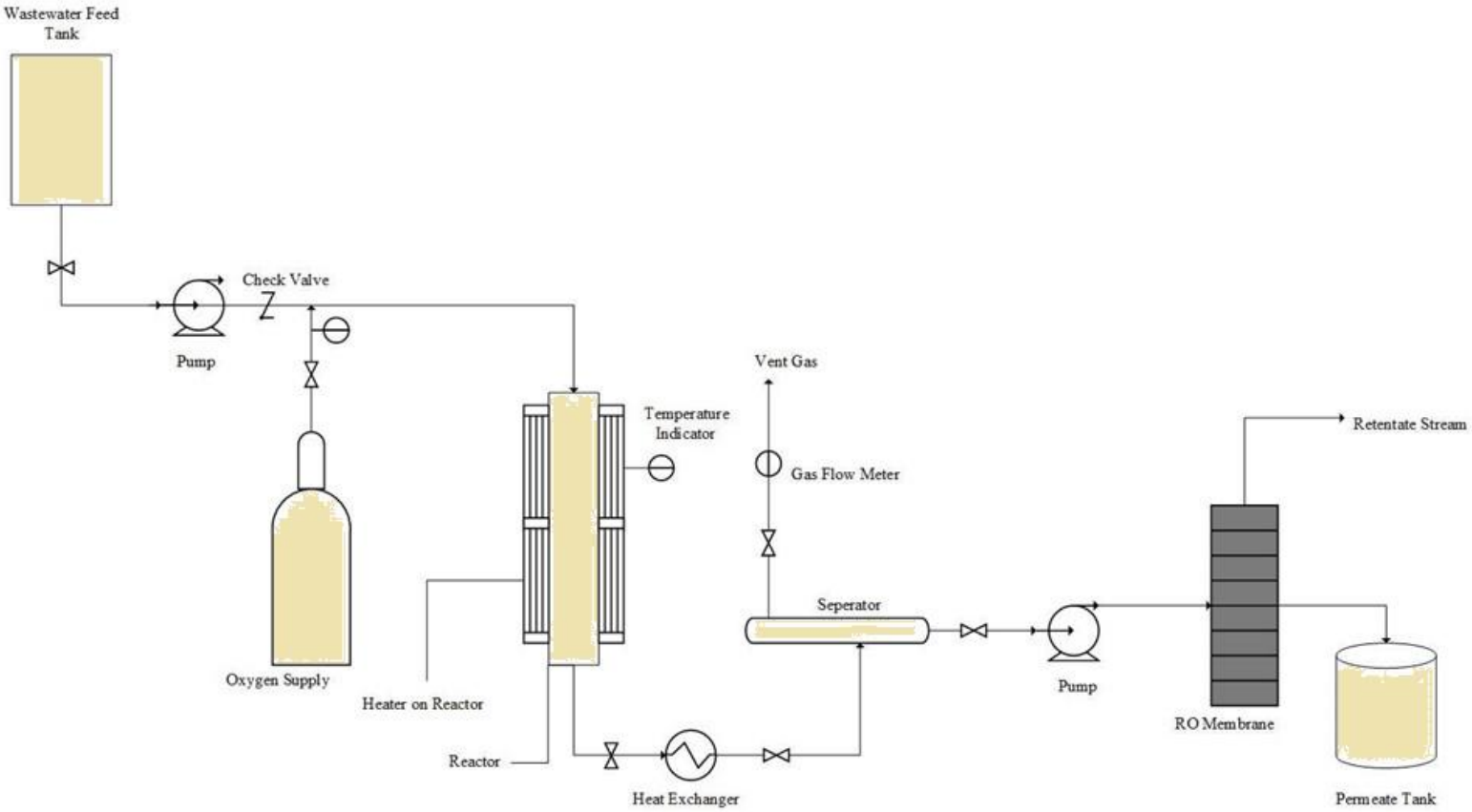

Fig. 1. Process flow diagram of the TBR-RO hybrid system (Adapted from Al-Obaidi et al., 2018a)

3. Modelling and validation of TBR and RO processes

The TBR and RO models are briefly described in this section.

3.1 TBR Modelling

The TBR model produced by Mohammed et al. (2016), shown in Appendix A, is used in this research with no changes made, as it consists of a multistage RO integrated with the TBR process.

The TBR model developed by Mohammed et al. (2016) includes a one-dimensional Langmuir-Hinshelwood based formulation. This is used to predict the performance of the reactor under the deployment of a catalyst (pt/γ-Al_2O_3) and pure oxygen as an oxidant. This model is essentially based on a set of ordinary algebraic and differential equations correlated with the thermos-physical properties of the system, as well as the associated mass and energy balances. The model is also based on the two-film theory and takes into consideration the chemical reaction rate of the mass and heat transfer of the process. Moreover, the TBR utilises a catalytic wet air oxidation (CWAO) process which adopts a plug flow model.

3.2 RO modelling

Quite a bit of research has been conducted on RO separation, however many of these use difficult simulations due to the complexity of RO modelling. The RO system is generally agreed to be challenging to model, due to the liquids needed to be separated which categorically rely on the membrane material. RO modelling in efficient, but readily available modelling software, is of great importance to advance the realm of RO research, which is why the gPROMS software has been selected for this work as it is vastly effective for RO based desalination process designs (Toth, 2020). Similar to Altaee (2012), the performance of the RO system was studied using a computational model and inputted into gPROMS; correspondingly, a commercial membrane manufacturing company is also considered here as seen in Table 1.

The multistage RO system was developed from the single membrane model by Al-Obaidi et al. (2018a), which can be seen in Appendix B. This is based on a one-dimensional spiral wound RO mathematical distribution model, which is used to estimate a variation of operating parameters across the x-axis of the membrane to produce an accurate phenolic rejection response from the aqueous solutions passing through the RO process. This model was used to investigate the thermo-physical properties of the system in relation to phenol, as well as the transport phenomena and spatial variation in the fluid properties.

The following assumptions are made for modelling the single RO membrane system as outlined by Al-Obaidi et al., (2017) and Al-Obaidi et al., (2018a):

1. The solution-diffusion model is adopted for the mass transfer of the solution through the membrane.
2. The membrane properties and the channel geometries are assumed to be constant.
3. The friction parameter in Darcy's law is used to characterise the pressure drops in the feed channel.
4. The permeate channel is assumed to retain constant atmospheric pressure during the process.
5. The solute concentration is assumed to be constant in the permeate channel, where the average values will be calculated from the inlet and outlet permeate solute concentrations.
6. The underlying process is assumed to be isothermal.

Al-Obaidi et al. (2018a) simulated the TBR and RO single stage model on gPROMS, where the RO and TBR systems were first modeled separately and validated against previous experimental data from literature. After checking that both systems were valid, the individual systems were integrated, modeled and simulated to form a hybrid system. An estimation of unknown parameters for the separate TBR process was done using gPROMS with the help of the gEST option on the software, where literature values were used to help predict unknown parameters for the RO system. These

unknown parameters were the water permeability constant, the phenol permeability constant, and the friction parameter of the RO process. A model validation was completed by creating a trend which showed that the model predictions were accurate. The model prediction results were also compared to the experimental data of the TBR system under numerous different operating conditions to attain the best possible phenol rejection rate. The model validation for the RO system was completed in five sets of inlet feed concentration and pressure, where observations were done using literature values to check if the predicted values were accurate. Al-Obaidi et al. (2018a) were able to validate the RO system by creating a trend to compare predicted values against experimental data values from literature with marginal differences. The model also assumed that the membrane lengths and the f-function are fully differentiable. The TBR system parameters were scaled up from literature, this is because most literature values assumed a small-scale laboratory system, whereas Al-Obaidi et al. (2018a) suggested following the literature plan of Mohammed et al. (2016) which scaled up for a large-scale industrial system. This involved the use of larger catalyst volumes and a much higher flowrate, which was found with the use of energy balances. Al-Obaidi et al. (2018a) modeled the same TBR scale- up operation conditions to that of Mohammed et al. (2016) which are: reactor length, inner reactor diameter, reactor volume, catalyst bed length, ratio of bed catalyst over inner reactor diameter, volume of catalyst, bed porosity, particle density, particle porosity.

This research has been developed from a single membrane RO and TBR hybrid system of Al-Obaidi et al. (2018a). However, a single stage system of an individual RO membrane will not suffice for real world applications in a large industrial scale plant. It is for this reason that this research attempts to discover the performance of a multistage approach to the RO segment of the hybrid system, to better accommodate a large-scale setting.

4. Multistage RO configurations

This section discusses multistage RO configurations and the modelling of multistage RO systems.

4.1 Multistage RO configurations

Parallel, series, tapered and permeate reprocessing configurations are described more particularly in this sub-section.

4.1.1 Parallel configuration

In this configuration (Fig. 2), the feed inlet stream splits into three separate streams in a parallel arrangement. This causes a lower flowrate in each RO membrane due to the splitting of the inlet flowrate. Consequently, the parallel configuration is arranged in such a way that all the membranes, not only receive about the same amount of feed flow, but they also operate at the same rates of recovery due to the same operating pressure. This configuration yields lower pressure losses across the stream of the membrane due to low feed flow rates. The parallel arrangement of the membranes can further attain high recovery rates in subsequent stages due to the high pressure and concentration in the streams (Al-Obaidi et al., 2018b). This configuration is widely attributed to its ability to handle higher throughputs than most configurations (Schwinge, 2004). The parallel membrane design also offers a low rate of scale formation on the RO membranes (Meriem et al., 2013). This design is therefore expected to offer higher water recovery rates due to the higher residence time of the fluid inside the membrane.

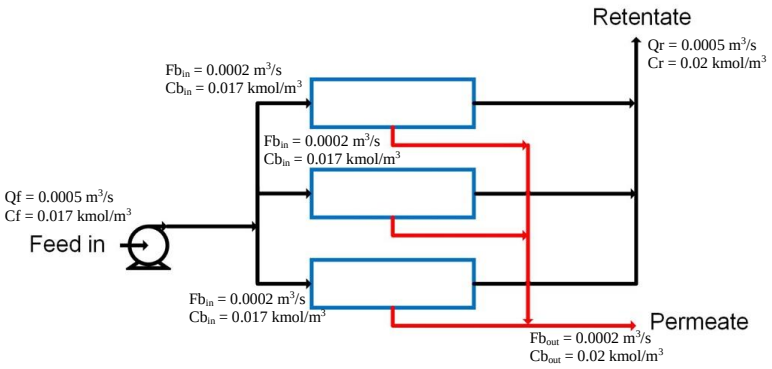

Fig. 2. RO parallel configuration

4.1.2 Series configuration

This configuration consists of three stages set in a series arrangement as depicted Fig. 3. It is restricted by high fouling in the feed, and its requirement for additional pump space at the feed. Although this configuration appears to offer a straightforward design, the implementation of this arrangement in practice can come as a challenge due to a lack of available space. However, even if space is available, the more the array length increases, the more the driving force decreases in the feed. This triggers an upsurge of feed concentration, which lowers the rate of mass transfer, and largely increases the rate of possible fouling in the system (Schwinge, 2004). The increase in length that the series array demands is also prone to producing high pressure drops across the feed channel, causing pressure loss and a driving force decrease for water permeation (Abbas, 2004; Carina et al., 2017). This configuration, nevertheless, is able to produce high water recovery rates due to the continuous reprocessing of the feed throughout the connected stages.

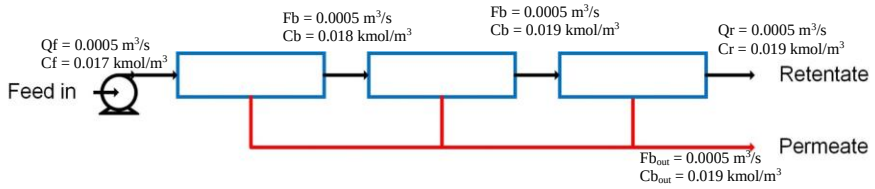

Fig. 3. RO series configuration

4.1.3 Tapered Configurations

The tapered configuration consists of a cascading number of parallel membrane units per stage. Fig. 4 and Fig. 5 show two proposed designs of tapered configurations, which have different impacts on the recovery of phenol but act quite similarly in respect to their phenol rejection. This phenomenon occurs because each configuration has a different effect on the inlet flowrate. This happens because the inlet feed stream splits into two for the first stage of the first configuration (Fig. 4) but does not split in the first stage of the second configuration (Fig. 5).

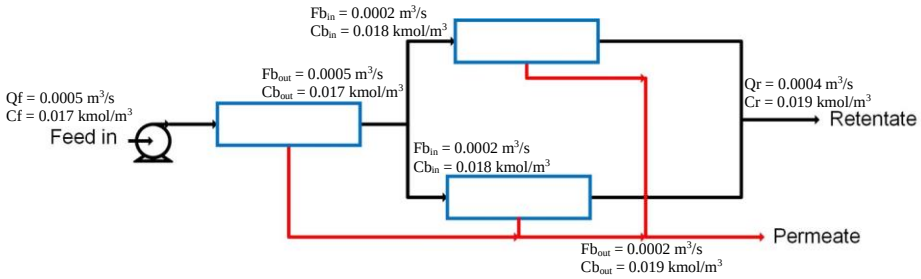

Fig. 4. RO tapered 1-2 configuration

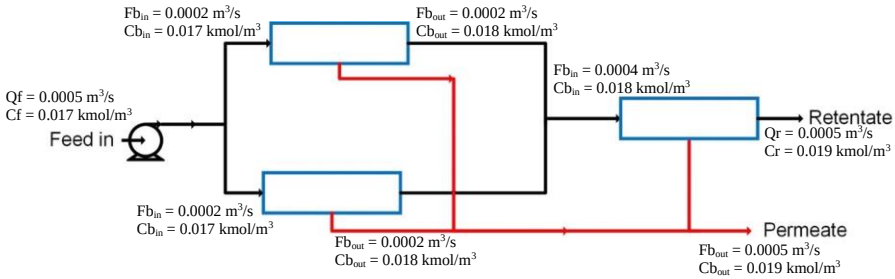

Fig. 5. RO tapered 2-1 configuration

Tapered configurations are very useful as their single pass configurations allow high recovery rates. However, low rejection rates, due to permeation (feed flowrate converted to permeate) are also associated with tapered configurations, hence causing an increase in the concentration polarisation. This in turn causes a precipitation of low soluble salts on the membrane surface, which affects the membrane characteristics and drastically decreases the permeate flux and solute rejection rate (Schwinge, 2004).

The tapered configuration is not restricted to low flowrates since the cascading effect of the stages causes a reduction in the cross-sectional area of the system, over the length of the system. This is proportional to the decreased areas of flowrate, which cause an increase in the overall flowrate. This configuration also usually requires the use of a high-pressured pump before the first stage, as the possible high retentate concentrations can readily decrease the pressure driving force in the streams

of the system. This is the reason why the addition of several pumps between each stage is sometimes deployed to increase the mass transfer of the system, as well as increase the overall system pressure (Schwinge, 2004).

4.1.4 Permeate reprocessing configuration

Similar to the tapered configuration, the permeate reprocessing configuration utilises a cascading number of membranes between each stage. The permeate 2:1 reprocessing configuration (Fig. 6) is where the membranes decrease in the sequential stage, going from two stages to one stage.

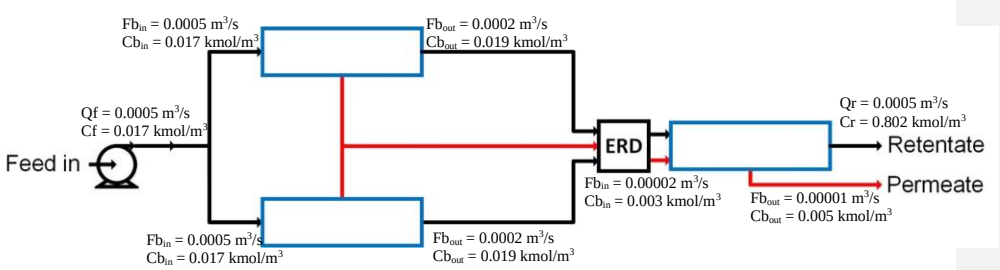

Fig. 6. Permeate 2:1 reprocessing configuration.

In this process, the permeate is collected from the membranes of the first stage and combined into one low-pressured stream to be fed into the subsequent stage. Similarly, the retentate is also collected from the first stage, but it is combined into a high-pressured stream. An energy recovery device (ERD) is then used between each stage, which absorbs surplus energy from the high pressured retentate stream and transfers it to the low pressured permeate stream. The ability of the ERD to effectively transfer energy is reliant on the efficiency of the device itself (Al-hotmani, 2020).

The permeate reprocessing design can be susceptible to low driving forces of pressure in the streams. However, the ERD is expected to regulate the pressure within the streams of the system. One of the consequences of such a design is the increased capital cost due to the ERD. Nonetheless, the advantages of acquiring a lower concentration of permeate at a lower energy consumption rate

outweighs the cost disadvantage. The operating costs of this system might be advantageous in the long run because of its energy saving properties.

4.2 Modelling of multistage RO systems

Five sub-models are generated for each of the five multistage RO configurations, as described in the previous sections. The sub-models are built around the specifications shown in Table 1. They include the reactor and catalyst properties used in the TBR process, as well as the membrane characteristics for the single membrane RO process, which were used to develop the multistage RO and TBR hybrid system simulated in the gPROMS software.

Table 1. TBR and RO specifications adapted from Al-Obaidi et al. (2018a)

Parameter	Value
Reactor Length	77 cm
Bed Catalyst Length (L_r)	30 cm
Inner Reactor Diameter (D_r)	1.9 cm
Catalyst Volume in Bed (V_{cat})	85 cm^3
Construction Material	Stainless Steel
Catalyst	(Pt/ -Al_2O_3)
Particle Shape	Sphere
Active Phase	(0.48 wt%) Pt
Support	
Calcination Temperature	400 °C
Bulk Density	0.647 (g/cm^3)
Pore Volume	0.308 (cm^3/g)
Particle Specific Surface Area (S_g)	259.9 (m^2/g)
Particle Diameter (d_{pe})	1.6 (mm)
Membrane:	
Supplier	Ion Exchange, India
Membrane Material and Module Configuration	TFC Polyamide, Spiral Wound
Feed Spacer Thickness (t_f)	0.85 mm
Effective Membrane Area (A)	0.75 m^2
Module Width (W)	1.6667 m
Module Length (L)	0.45 m
Module Diameter	0.0635 m

4.2.1 Sub-model of parallel configuration

The feed pressure, retentate flowrate, outlet feed pressure, retentate concentration, feed flowrate, feed concentration, and permeate flowrate are calculated using Eqs. 1 – 7, respectively. In this regard, RI01, R102, and so on, denote the stage number.

$$Pf_{plant} = R101.Pb_{inlet} \quad (1)$$

$$Qr_{plant} = 3 \times R101.Fb_{outlet} \quad (2)$$

$$Pf_{out\_plant} = R101.Pb_{outlet} \quad (3)$$

$$Cr_{plant} = R101.Cb_{outlet} \quad (4)$$

$$Qf_{plant} = R101.Fb_{inlet} \quad (5)$$

$$Cf_{plant} = R101.Cb_{inlet} \quad (6)$$

$$Qp_{plant} = 3 \times R101.Fp_{Total} \quad (7)$$

The permeate concentration can be calculated using the following equation:

$$Cp_{plant} = \frac{\left((R101.Fp_{Total} \times R101.Cp_{Avg}) + (R101.Fp_{Total} \times R101.Cp_{Avg}) + (R101.Fp_{Total} \times R101.Cp_{Avg})\right)}{Qp_{plant}} \quad (8)$$

The total rejection and the total recovery can be calculated using Eqs. 9, and 10, respectively.

$$SR_{plant} = (1 - (\frac{Cp_{plant}}{Cf_{plant}})) \times 100 \quad (9)$$

$$WR_{plant} = (\frac{Qp_{plant}}{Qf_{plant}}) \times 100 \quad (10)$$

While the pressure loss of the plant can be calculated using Eq. 11.

$$Pressure_{loss\_plant} = Pf_{plant} - R101.Pb_{outlet} \quad (11)$$

Eq. 12 can be used to calculate the specific energy consumption without ERD measured by kWh/m^3

$$POWER_{consumption_{pump}} = \frac{((Pf_{plant} \times 101325) \times Qf_{plant})}{(eff_{pump} \times Qp_{plant})} \over 36E5 \quad (12)$$

4.2.2. Series configuration sub-model

Eqs. 13 – 18 are used to describe the functionality of the respective configuration being simulated:

$$R102.Fb_{inlet} = R101.Fb_{outlet} \quad (13)$$

$$R102.Cb_{inlet} = R101.Cb_{outlet} \quad (14)$$

$$R102.Pb_{inlet} = R101.Pb_{outlet} \quad (15)$$

$$R103.Fb_{inlet} = R102.Fb_{outlet} \quad (16)$$

$$R103.Cb_{inlet} = R102.Cb_{outlet} \quad (17)$$

$$R103.Pb_{inlet} = R102.Pb_{outlet} \quad (18)$$

The retentate flowrate, retentate pressure, retentate concentration, and permeate flowrate are calculated using Eqs. 19 – 23, respectively.

$$Qr_{plant} = R103.Fb_{outlet} \quad (19)$$

$$Pf_{outplant} = R103.Pb_{outlet} \quad (20)$$

$$Cr_{plant} = R103.Cb_{outlet} \quad (21)$$

$$Qp_{plant} = R101.Fp_{Total} + R102.Fp_{Total} + R103.Fp_{Total} \quad (22)$$

The permeate concentration can be calculated using Eq. 23.

$$Cp_{plant} = \frac{\left(\left(R101.Fp_{Total} \times R101.Cp_{Avg}\right) + \left(R102.Fp_{Total} \times R102.Cp_{Avg}\right) + \left(R103.Fp_{Total} \times R103.Cp_{Avg}\right)\right)}{Qp_{plant}} \quad (23)$$

The total rejection, the total recovery, and specific energy consumption without ERD measured in kWh/m^3 can be calculated using Eqs. 9, 10, and 12, respectively. However, the pressure loss of the plant can be calculated using Eq. 24.

$$Pressure_{loss\_plant} = Pf_{plant} - R103.Pb_{outlet} \quad (24)$$

4.2.3. Sub-model of tapered 1:2 configuration

The characteristics of the proposed configuration are found in Eqs. 25 – 27.

$$R102.Fb_{inlet} = 0.5 \times R101.Fb_{outlet} \quad (25)$$

$$R102.Cb_{inlet} = R101.Cb_{outlet} \quad (26)$$

$$R102.Pb_{inlet} = R101.Pb_{outlet} \quad (27)$$

The retentate flowrate, and retentate pressure, are calculated using Eqs. 28 – 29, respectively.

$$Qr_{plant} = 2 \times (R102.Fb_{outlet}) \quad (28)$$

$$Pf_{outplant} = R102.Pb_{outlet} \quad (29)$$

The retentate concentration, feed flowrate, feed concentration, permeate flowrate, and permeate concentration are calculated using Eqs. 30 – 34, respectively.

$$Cr_{plant} = R102.Cb_{outlet} \quad (30)$$

$$Qf_{plant} = R101.Fb_{inlet} \quad (31)$$

$$Cf_{plant} = R101.Cb_{inlet} \quad (32)$$

$$Qp_{plant} = (R101.Fp_{Total} + 2) \times (R102.Fp_{Total}) \quad (33)$$

$$Cp_{plant} = \frac{((R101.Fp_{Total} \times R101.Cp_{Avg}) + (2 \times (R102.Fp_{Total} \times R102.Cp_{Avg}))}{Qp_{plant}} \quad (34)$$

Similarly, the total rejection, the total recovery, and specific energy consumption without ERD measured in kWh/m^3 can be calculated using Eqs. 9, 10, and 12, respectively. The total pressure loss can be calculated using Eq. 35.

$$Pressure_{loss\_plant} = Pf_{plant} - R102.Pb_{outlet} \quad (35)$$

4.2.4. Tapered 2_1 configuration sub-model

The characteristics of the proposed configuration are found in Eqs. 36 – 38, where the functionality of the respective configuration is translated to the system.

$$R102.Fb_{inlet} = 2 \times R101.Fb_{outlet} \quad (36)$$

$$R102.Cb_{inlet} = R101.Cb_{outlet} \quad (37)$$

$$R102.Pb_{inlet} = R101.Pb_{outlet} \quad (38)$$

The retentate flowrate, and retentate pressure, are calculated using Eqs. 39 and 40, respectively.

$$Qr_{plant} = R102.Fb_{outlet} \quad (39)$$

$$Pf\_out_{plant} = R102.Pb_{outlet} \quad (40)$$

The retentate concentration, permeate flowrate, and permeate concentration are calculated using Eqs. 41 – 43, respectively.

$$Cr_{plant} = R102.Cb_{outlet} \quad (41)$$

$$Qp_{plant} = (2 \times R101.Fp_{Total}) + R102.Fp_{Total} \quad (42)$$

$$Cp_{plant} = \frac{((2\times(R101.Fp_{Total}\times R101.Cp_{Avg}))+(R102.Fp_{Total}\times R102.Cp_{Avg}))}{Qp_{plant}} \quad (43)$$

The total rejection, the total recovery, and specific energy consumption without the ERD and measured in kWh/m^3 can be calculated using Eqs. 9, 10, and 12, respectively. However, the total pressure drop is calculated using Eq. 44.

$$Pressure_{loss\_plant} = Pf_{plant} - R102.Pb_{outlet} \quad (44)$$

4.2. Permeate reprocessing 2_1 configuration sub-model

The characteristics of the proposed configuration are found in Eqs. 45 – 47, where the functionality of the respective configuration is translated to the system.

$$R102.Fb_{inlet} = 2 \times (R101.Fp_{total}) \quad (45)$$

$$R102.Cb_{inlet} = R101.Cp_{avg} \quad (46)$$

$$R102.Pb_{inlet} = R101.Pb_{outlet} \times eff\_erd \quad (47)$$

The retentate flowrate, and retentate pressure, are calculated using Eqs. 48 and 49, respectively.

$$Qr_{plant} = R102.Fb_{outlet} + (2 \times R101.Fb_{outlet}) \quad (48)$$

$$Pf_{out_{plant}} = R102.Pb_{outlet} \quad (49)$$

The retentate concentration, feed flowrate, feed concentration, permeate flowrate and permeate concentration are calculated using Eqs. 50 – 54, respectively.

$$Cr_{plant} \times Qr_{plant} = (R102.Cb_{outlet} \times R102.Cb_{outlet}) + (R101.Cb_{outlet} \times R101.Cb_{outlet}) \quad (50)$$

$$Qf_{plant} = 2 \times R101.Fb_{inlet} \quad (51)$$

$$Cf_{plant} = R101.Cb_{inlet} \quad (52)$$

$$Qp_{plant} = R102.Fp_{Total} \quad (53)$$

$$Cp_{plant} = \frac{(R102.Fp_{Total} \times R102.Cp_{Avg})}{Qp_{plant}} \quad (54)$$

The total rejection, the total recovery, and specific energy consumption without ERD measured in kWh/m^3 can be calculated using Eqs. 9, 10, and 12, respectively. The pressure loss of the plant is calculated using Eq. 55.

$$Pressure_{loss\_plant} = Pf_{plant} - R102.Pb_{outlet} \quad (55)$$

5. Evaluation of hybrid systems of TBR and multistage RO configurations

This section presents the results of the five TBR and multistage RO hybrid systems with the aim of identifying which TBR-multistage RO combination would yield the best results. A detailed analysis will be carried out to assess the influence of a set of inlet conditions on the performance indicators of each of the hybrid system combinations.

The operating conditions for the hybrid TBR-Multistage RO are shown in Table 2, along with the total membrane area for each case. The results in Table 3 depict the TBR and multistage RO hybrid systems, which were simulated using the gPROMS software. For the purposes of comparison, Table 3 shows a summary of the results obtained by Al-Obaidi et al. (2018a) where a hybrid TBR-single RO membrane of 0.75 m^2 is used (Table 1). Table 4 shows the permeate concentration for each case including that obtained by Al-Obaidi et al. (2018).

The results clearly depict that the permeate reprocessing configuration with a 2:1 stage was the best multistage option, as it gave the highest phenol rejection rate, in the ranges of 96.78 –99.46%, as well as the highest benefit percentage, 22.10–58.16 %. These ranges are higher than the single membrane RO and TBR hybrid system (Al-Obaidi et al., 2018a), where the phenol rejection rate was between

95.38–99.15% and a benefit percentage between 4.32–55%. There is a noticeable improvement in the benefit percentages where previously the minimum benefit was 4.32%, whereas with the new hybrid configuration, it is 22.10%. The maximum benefit also increased from 55% to 58.16%.

Similar to the single membrane RO process (Table 2), the multi-stage process (Table 3) shows that the inlet phenol flowrate and concentration have little effect on the phenol rejection, as there is only a slight increase in phenol rejection when these two parameters increase (Case 1-9). This is also confirmed by Al-Obaidi et al. (2018a), where the authors stated that there is little to no impact of the inlet feed flowrate and concentration on the rejection rates. However, looking at Cases 3 and 4 in Table 2, it is evident that when both the inlet feed concentration and the inlet feed flowrate increase, the phenol rejection also increases in the RO. This is also validated in Table 3 in Cases 4 and 5, which show a similar outcome. This phenomenon starts with an increase in the inlet concentrations, which in turn increases the membrane solute isolation intensity. As a result, the concentration polarisation decreases, and finally an increase in the feed flowrate is observed (Al-Obaidi et al., 2018a).

It is for this reason that the rejection rate varies from case to case. The 2:1 permeate reprocessing configuration produced the highest rates of phenol rejection, when coupled with the TBR (99.84%), with a 58.16% increased benefit of the two systems working together, rather than individually. The permeate 2:1 reprocessing configuration was successful because the permeate stream was at a lower pressure, which naturally happens in RO processes. However, this disadvantage was resolved with the help of an energy reprocessing device (ERD), which redirects energy from the high pressured retentate stream to the low pressured permeate stream, thus providing more energy in the permeate stream.

Since, RO is a pressure driven process, a high amount of pressure is needed to combat the osmotic pressure on the retentate side. The high pressure increases the water flux, thus slightly increasing the total permeate recovery, and finally causing a high phenol rejection rate. Although, the total permeate recovery might not seem to be as high as the other recovery rates, nor does it seem to give a large product capacity, it does however produce the best quality water. The way that the permeate

reprocessing design is arranged, gives it an advantage over the other five configurations. This is because the cascading effect of the arranged stages, prevent the prevalence of a low flowrate; this is ideal in theory, but in reality, it can contribute to a higher specific energy consumption (SEC). This configuration is also sometimes prone to high retentate concentrations, as the driving force can decrease as a result. This is also why the ERD is important, as it can combat the occurrence of a low driving force. The implementation of an ERD between each stage increases the bulk velocity and Reynolds numbers, which causes the mass transfer coefficient to increase. When this happens, there is a higher water flux which is proportional to a higher phenol rejection rate.

Table 2. Operating conditions of TBR and RO process

Case	TBR process					RO process		
	Inlet feed flow rate (m^3/h)	Inlet phenol concentration (ppm)	Reaction temperature (°C)	Oxygen partial pressure (atm)	Gas flowrate (%)	Inlet feed concentration (ppm)	Inlet feed flowrate (m^3/h)	Membrane areas
1	0.58	5000	120	7.90	80	563.96	0.58	1. Hybrid TBR-Single membrane RO (Al-Obaidi et al, 2018a) = 0.75 m^2 2. TBR-Multistage Series RO hybrid system = 2.25 m^2 3. TBR-Multistage Parallel RO hybrid system = 2.25 m^2 4. TBR-Multistage Tapered 1_2 RO hybrid system = 2.25 m^2 5. TBR-Multistage Tapered 2_1 hybrid system = 2.25 m^2 6. TBR-Multistage Permeate 2_1 RO hybrid system = 2.25 m^2
2	0.58	5000	140	7.90	80	448.05	0.58	
3	0.58	5000	160	7.90	80	333.47	0.58	
4	1.16	5000	120	7.90	80	1260.56	1.16	
5	1.16	5000	140	7. 90	80	1014.72	1.16	
6	1.16	5000	160	7. 90	80	777.25	1.16	
7	1.74	5000	120	7. 90	80	1940.52	1.74	
8	1.74	5000	140	7. 90	80	1628.32	1.74	
9	1.74	5000	160	7. 90	80	1317.80	1.74	
10	0.58	5000	160	7. 90	80	333.47	0.58	
11	0.58	5000	160	9. 90	80	282.52	0.58	
12	0.58	5000	160	11.84	80	260.95	0.58	
13	0.58	1000	160	11.84	80	185.43	0.58	
14	0.58	3000	160	11.84	80	222.57	0.58	
15	0.58	5000	160	11.84	80	248.24	0.58	
16	0.58	5000	140	7.90	20	448.07	0.58	
17	1.16	5000	140	7.90	20	1014.76	1.16	
18	1.74	5000	140	7.90	20	1628.35	1.74	
19	0.58	5000	140	7.90	40	448.06	0.58	
20	1.16	5000	140	7.90	40	1014.74	1.16	
21	1.74	5000	140	7.90	40	1628.34	1.74	
22	0.58	5000	140	7.90	80	448.05	0.58	
23	1.16	5000	140	7.90	80	1014.72	1.16	
24	1.74	5000	140	7.90	80	1628.32	1.74	
25	0.58	5000	140	7.90	100	448.05	0.58	
26	1.16	5000	140	7.90	100	1014.72	1.16	
27	1.74	5000	140	7.90	100	1628.31	1.74	

*Fixed inlet feed pressure and temperature are 14.8 atm and 34 °C, respectively

Table 3. Results of the multistage RO and TBR hybrid system compared with the results of a single membrane RO and TBR hybrid system developed by Al-Obaidi et al. (2018a)

		Results of single stage hybrid system by Al-Obaidi et al., (2018a)				TBR-Multistage Series RO hybrid system		TBR-Multistage Parallel RO hybrid system		TBR-Multistage Tapered 1_2 RO hybrid system		TBR-Multistage Tapered 2_1 RO hybrid system		TBR-Multistage Permeate 2_1 RO hybrid system	
		Individual TBR system	Individual RO system	TBR- Single stage RO hybrid system											
Case	Inlet feed flow rate (m^3/h)	% Phenol rejection (-)	% Phenol rejection (-)	% Phenol rejection (-)	% Benefit	% Phenol rejection (-)	% Benefit	% Phenol rejection (-)	% Benefit	% Phenol rejection (-)	% Benefit	Phenol rejection (-)	% Benefit	% Phenol rejection (-)	% Benefit
1	0.58	88.72	82.90	98.07	10.54	97.78	10.21	96.37	8.62	97.28	9.65	97.27	9.64	98.36	10.86
2	0.58	91.04	82.87	98.46	8.15	98.23	7.90	97.08	6.64	97.83	7.46	97.82	7.45	98.69	8.41
3	0.58	93.33	82.83	98.85	5.92	98.68	5.73	97.80	4.79	98.37	5.40	98.37	5.40	99.02	6.10
4	1.16	74.79	86.82	96.68	29.26	96.39	28.89	94.88	26.86	95.95	28.29	95.86	28.18	97.51	30.38
5	1.16	79.71	86.82	97.33	22.10	97.10	21.82	95.84	20.25	96.73	21.36	96.66	21.27	98.00	22.96
6	1.16	84.45	86.82	97.95	15.98	97.78	15.78	96.79	14.61	97.49	15.44	97.43	15.37	98.47	16.60
7	1.74	61.19	88.11	**95.38**	**55.88**	94.81	54.95	**93.50**	**52.80**	**94.57**	**54.55**	**94.52**	**54.47**	**96.78**	**58.16**
8	1.74	67.43	88.14	96.14	42.56	95.67	41.87	94.52	40.17	95.45	41.55	95.40	41.47	97.32	44.32
9	1.74	73.64	88.16	96.88	31.55	96.51	31.05	95.55	29.75	96.32	30.80	96.28	30.73	97.84	32.86
10	0.58	93.33	82.83	98.85	5.92	98.68	5.73	97.80	4.79	98.37	5.40	98.37	5.40	99.02	6.10
11	0.58	94.35	82.80	99.03	4.96	98.88	4.80	98.12	4.00	98.62	4.52	98.61	4.52	99.17	5.11
12	0.58	94.78	82.80	99.10	4.56	98.96	4.41	98.26	3.67	98.72	4.16	98.72	4.15	99.24	4.70
13	0.58	81.46	82.77	96.81	18.84	99.26	21.86	**98.75**	**21.24**	**99.08**	**21.64**	**99.08**	**21.64**	**99.46**	**22.10**
14	0.58	92.58	82.79	98.72	6.63	99.11	7.06	98.51	6.41	98.90	6.83	98.90	6.83	99.35	7.31
15	0.58	95.04	82.80	99.15	4.32	99.01	4.18	98.34	3.48	98.78	3.94	98.78	3.94	99.27	4.46
16	0.58	91.04	82.87	98.46	8.15	98.23	7.90	97.08	6.64	97.83	7.46	97.82	7.45	98.69	8.41
17	1.16	79.70	86.82	97.33	22.10	97.10	21.83	95.84	20.25	96.73	21.36	96.66	21.27	98.00	22.96
18	1.74	67.43	88.14	96.14	42.56	95.67	41.87	94.52	40.18	95.45	41.55	95.40	41.48	97.32	44.32
19	0.58	91.04	82.87	98.46	8.16	98.23	7.90	97.08	6.64	97.83	7.46	97.82	7.45	98.69	8.41
20	1.16	79.71	86.82	97.33	22.10	97.10	21.82	95.84	20.25	96.73	21.36	96.66	21.27	98.00	22.96
21	1.74	67.43	88.14	96.14	42.56	95.67	41.87	94.52	40.17	95.45	41.55	95.40	41.47	97.32	44.32
22	0.58	91.04	82.87	98.46	8.15	98.23	7.90	97.08	6.64	97.83	7.46	97.82	7.45	98.69	8.41
23	1.16	79.71	86.82	97.33	22.10	97.10	21.82	95.84	20.25	96.73	21.36	96.66	21.27	98.00	22.96
24	1.74	67.43	88.14	96.14	42.56	95.67	41.87	94.52	40.17	95.45	41.55	95.40	41.47	97.32	44.32
25	0.58	91.04	82.87	98.46	8.15	98.23	7.90	97.08	6.64	97.83	7.46	97.82	7.45	98.69	8.41

26	1.16	79.71	86.82	97.33	22.10	97.10	21.82	95.84	20.25	96.73	21.36	96.66	21.27	98.00	22.96
27	1.74	67.43	88.14	96.14	42.56	95.67	41.80	94.52	40.17	95.45	41.55	95.40	41.47	97.32	44.32

* Fixed inlet feed pressure Pb (0) and temperature TRO of RO process are 14.8 atm and 34°C, respectively.

Table 4. Permeate Concentration of the multistage RO-TBR hybrid system and the single membrane RO-TBR hybrid system with varying pressure

	Single Stage RO and TBR hybrid system	Multistage Stage RO and TBR hybrid systems				
		TBR-Multistage Series RO hybrid system	TBR-Multistage Parallel RO hybrid system	TBR-Multistage Tapered 1_2 RO hybrid system	TBR-Multistage Tapered 2_1 RO hybrid system	TBR-Multistage Permeate 2_1 RO hybrid system
Pressure	Permeate Concentration (ppm)					
10.8	218.77	279.04	268.78	257.01	246.00	160.93
11.8	209.01	254.19	267.18	244.69	238.48	173.16
12.8	201.89	237.16	270.00	236.31	233.77	139.28
13.8	196.77	225.11	270.00	230.85	231.04	133.64
14.8	193.19	216.55	273.77	227.56	230.01	134.58
15.8	190.84	210.43	278.94	226.15	230.29	136.46
16.8	189.51	206.29	285.25	226.05	231.70	140.22
17.8	189.02	203.65	292.68	227.18	234.15	144.93
18.8	189.26	202.24	300.96	229.35	237.44	150.58

6. Evaluation of hybrid system using pressure variation

The results of the hybrid system, obtained in Table 3, need to be investigated further prior to implementation. A study of pressure variation was therefore conducted against four performance metrics, namely, specific energy consumption, permeate concentration, phenol rejection, and permeate recovery. Pressure was chosen as an independent variable to characterise the hybrid system, due to its direct impact on the four mentioned metrics, as well as the fact that reserve osmosis is a pressure driven process.

6.1 Effect of pressure on rejection

The results shown graphically in Fig. 7 corroborate with those already discussed in Section 5, where it was affirmed that the permeate 2:1 configuration had the highest rejection, and the parallel configuration had the lowest. From Fig. 7, it seems that most of the configurations observe a decline in the rejection as the pressure increases. This is true with the exception of the single and series configurations, which continue to decrease. This is because the majority of the configurations operate at an optimum pressure of around 14.8 atm.

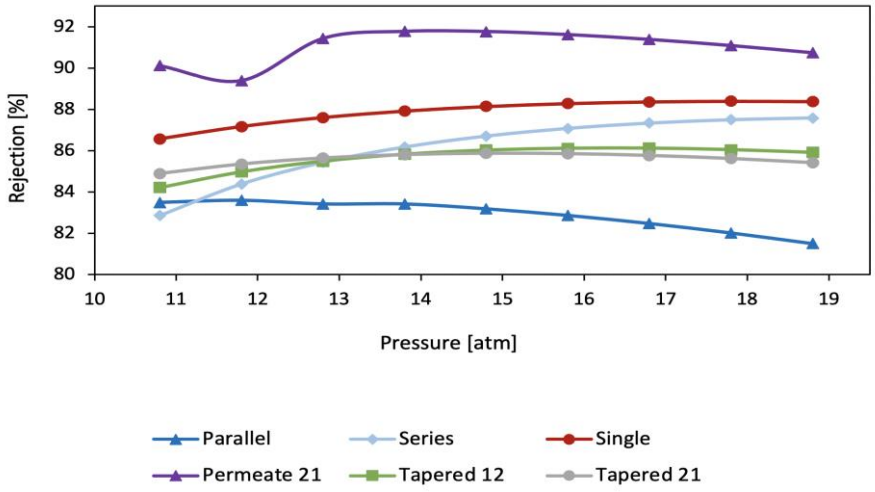

Fig. 7. The effect of applied pressure on phenol rejection for five multistage configurations and single membrane

6.2 Effect of pressure on permeate concentration (Cp)

Fig. 8 graphically illustrates the relationship between the pressure and permeate concentration, which shows a clear distinction between the permeate 2:1 configuration and the rest of the configurations. It is evident that the permeate 2:1 arrangement yields the best permeate concentration, which in turn corresponds to a better phenol rejection. This is made clear in Fig. 7, which displays the relationship of the permeate concentration and the phenol rejection, where the Cp sometimes shares an inversely proportional relationship with salt rejection.

The low Cp of the permeate 2:1 configuration in Fig. 8 is attributed to a high permeate flux, where as the feed pressure increases, the dilution increases, which finally allows an increase in the permeation of the feed (Al-Obaidi et al., 2018b).

Commented [JAH1]: Where as – not whereas (two words separately).

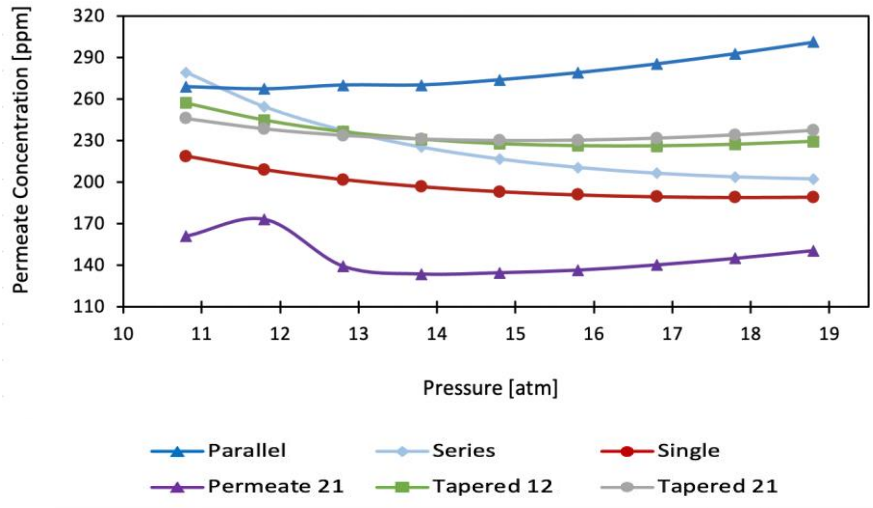

Fig. 8. The effect of pressure on permeate concentration for five multistage configurations and single membrane

6.3. Effect of pressure on water recovery

Fig. 9 depicts the relationship existing between the pressure and water recovery, where as the pressure and permeate flowrate increase, the water recovery increases as well. In this regard, the parallel configuration seems to yield a higher water recovery. This starts by the feed flowrate going into the parallel membranes and splitting equally between each membrane compartment. This means that the flowrate then decreases, which calls for a higher membrane residence time. When the stream spends more time in the membrane, it allows a higher filtration rate and a higher water flux. When this happens, a higher permeate flowrate is observed, finally resulting in a higher recovery.

Although the parallel configuration yields a high water recovery rate, it rejects the least amount of phenol as previously seen in Fig. 8. This is because high recovery rates are usually associated with high salt concentrations, which is why the rejection performance of the parallel configuration is so low. Higher water recovery rates are also more prone to pre-disposal treatments, which would not be very beneficial to industries. To overcome this, a higher pressure must be implemented in the parallel configuration, in order to overcome the osmotic pressures.

Commented [JAH2]: "where as" rather than whereas. Two words separately.

While lower water recovery can correspond to lower product capacity, low recovery processes produce reject-water streams that are safe enough to be used for bathroom use and general washing. The main limitations of membrane designs result in a low water recovery feasibility, as well as concentration polarisation, membrane fouling and hydraulic resistance to the permeate flow rate. The water recovery can be increased, while keeping salt concentrations low, by improving the overall membrane performance, and increasing the feed water temperature (Gude, 2011).

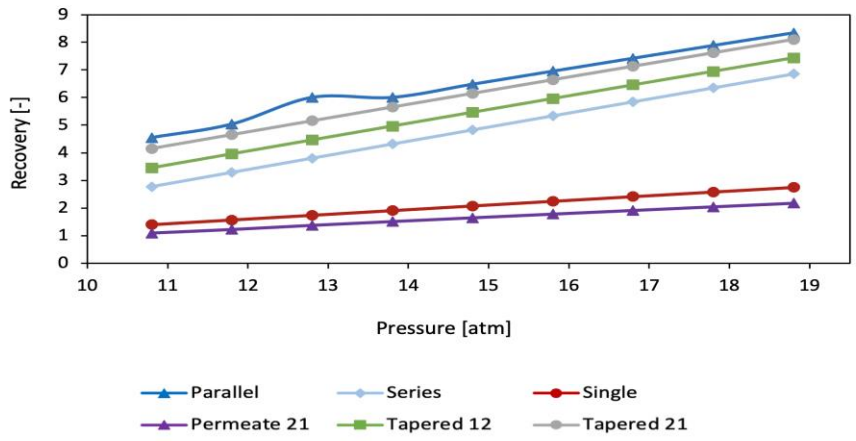

Fig. 9. Effect of pressure on water recovery (yield) for five multistage configurations and single membrane

6.4. Effect of pressure on specific energy consumption (SEC)

The effect of a varying inlet feed pressure at a constant inlet feed flowrate of 4.833E-4 m^3/s, and a constant temperature of 34 ºC is shown in Fig. 10. It is evident that the SEC decreases as the pressure increases. This happens because at high pressures, the volume of water needing pressurisation is low.

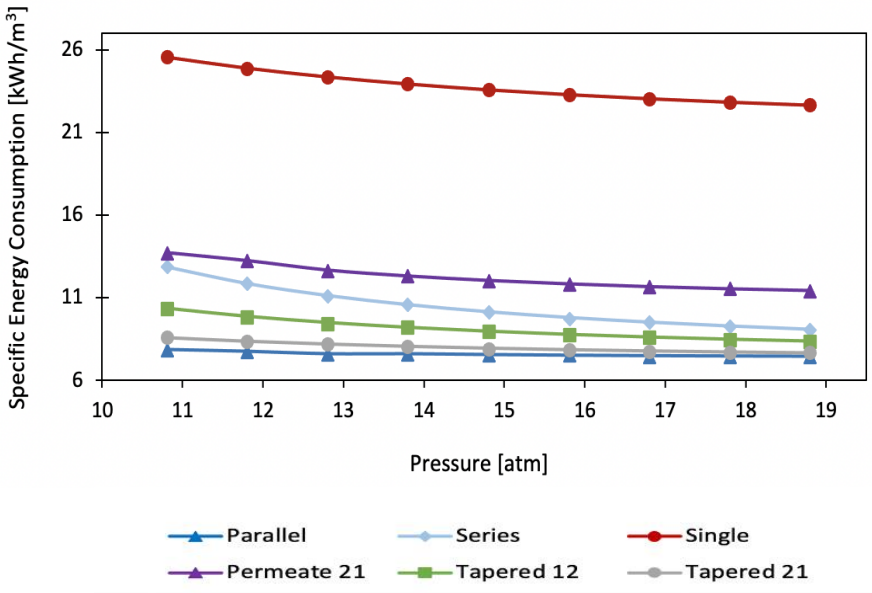

Fig. 10. Effect of pressure on SEC for five multistage configurations and single membrane

Although Table 3 confirms that the 2:1 permeate arrangement is able to achieve the most effective phenol rejection rate, the results in Fig. 10 show that it consumes a greater amount of specific energy in comparison with the rest of the multistage configurations. Nevertheless, the amount of energy consumed by all of the multistage configurations (7 kWh/m^3 to 13 kWh/m^3) is far less than the energy consumed by the single stage configuration (22 kWh/m^3 to 25 kWh/m^3) as indicated by Al-Obaidi et al. (2018a). It seems that the parallel configuration consumes the least energy due to the way the feed flowrate is split, leading to a reduced flowrate in each membrane compartment, which in turn causes an increased residence time for the feed in each membrane. This means that the streams will have a longer filtration process, where the permeate flowrate will increase, as well as the product capacity and recovery, and finally the SEC decreases (Al-Obaidi et al., 2018c).

The reason why the 2:1 permeate arrangement consumes more energy, compared to the other multistage configurations, is because of the increase in flowrate caused by the ERD, which causes pressure losses due to friction across the length of the membrane. This lowers the average osmotic

pressure and concentration polarisation, finally causing a decreased permeate recovery and an increased SEC, but also providing the most phenol rejection, and the highest quality of permeate. (Chakraborty et al., 2020; Al-Obaidi et al., 2018c).

In addition, the simulation results (Fig. 10) reveal that a greater Cp will usually account for a lower energy consumption, as obtained by the parallel configuration. The same findings were demonstrated by Chakraborty et al. (2020). Evidently, a lower Cp as observed in the 2:1 permeate configuration, will yield a higher SEC, as illustrated in Fig. 10.

Table 4 further supports this analogy by showing the significant decrease of Cp corresponding to the 2:1 permeate configuration, as the pressure increases. The two tapered configurations are shown to observe a much slower decrease rate in the Cp than the series configuration, meanwhile the parallel configuration observes an anomalous increase. The same table clearly depicts the low Cp values, obtained by the 2:1 permeate configuration, which is commensurate with the higher multistage SEC values shown in Fig. 10.

The multistage RO and TBR systems seem to produce promising outcomes when put together. As seen in the research, a substantial amount of benefit is generated when working together rather than individually, which corresponds to high rejection rates. For this reason, it is believed that the researched multistage RO and TBR hybrid process can be used in an industrial scale setting.

7. Conclusions

This paper has presented a pilot-scale hybrid system based on a multistage reverse osmosis process coupled with a trickle bed reactor. This multistage hybrid system is of a novel technology that has not been implemented or researched in the past; the two systems have been hybridized and designed to mitigate the presence of phenol in industrial wastewater, using the lowest possible energy consumption. The characteristics of this novel TBR and multistage RO system have proved the feasibility of this system as an efficient industrial design compared to the hybrid system of TBR and single membrane RO process developed in the literature.

This has been achieved using five different multistage configurations for the RO process, which were modelled and simulated on the gPROMS software. The study focused on the effects of pressure on four performance metrics: specific energy consumption, permeate concentration, phenol rejection, and permeate recovery. The highest phenol rejection rate was achieved using the 2:1 permeate reprocessing configuration. This configuration led to improved phenol rejection results due the use of an ERD which increased the water flux in the stream and transferred energy from the high-pressured retentate stream to the low-pressured permeate stream. However, the 2:1 permeate reprocessing configuration had a few predicaments due to the natural limitations of membranes. These predicaments are restraints such as a considerable amount of specific energy consumption, and a low water recovery. However, the results of the 2:1 permeate reprocessing design show that the multistage RO had a 58% benefit, in comparison to the 55% benefit attained for the single membrane RO. Similarly, the proposed multistage design had a rejection rate of 99.46%, in comparison with 99.15% for the single membrane RO. Additionally, there appears to be a significant difference here in terms of the benefits, where previously the lowest benefit achieved was 4% in the single stage RO and TBR hybrid system from literature, however, the multistage configuration yields a minimum benefit of 22%. The work presented can be of significant importance when it is implemented in a real-world application, as a single membrane RO design will not suffice for many industrial scale applications. Future work along similar lines has already started to achieve even higher benefits and pollutant rejection rates, as well as a lower SEC.

Nomenclature

A	[m^2]	The effective membrane area of the RO
Aw	[m/atm s]	The solvent transport coefficient of the RO membrane
A^0	[$mol/cm^3]^{1-n}$ s^{-1}	The pre-exponential factor of the TBR system
aGL	[cm^{-1}]	The specific gas-liquid contact area per unit volume of bed of the TBR
aLS	[cm^{-1}]	The specific liquid-solid contact area per unit volume of bed of the TBR
b	[atm s/m^4]	The friction parameter of the feed and permeate channels in the RO
Bs	[m/s]	The solute transport coefficient of the RO system
B_b	[kg/m^3]	The concentration of the bulk phenol in the feed
$Cb(x)$	[kg/m^3]	The phenol concentration of the feed channel at any point across the x-axis of the RO
$Cb(0)$	[kg/m^3]	The inlet phenol concentration of the RO feed channel
$Cb(L)$	[kg/m^3]	The outlet phenol concentration of the RO feed channel
$CO2$	[mol/cm^3]	The concentration of the oxygen in the TBR
$CO2,G$	[mol/cm^3]	The concentration of oxygen in the gas phase of the TBR
$CO2,L$	[mol/cm^3]	The concentration of oxygen in the liquid phase of the TBR
$CO2,L-S$	[mol/cm^3]	The concentration of oxygen in the liquid-solid interface of the TBR
$Cp(av)$	[$kmol/m^3$]	The average permeate phenol concentration in the RO permeate channel
$Cp(0)$	[$kmol/m^3$]	The inlet permeate phenol concentration in the RO permeate channel
$Cp(L)$	[$kmol/m^3$]	The outlet permeate phenol concentration in the RO permeate channel
$Cp\mathrm{h}$	[mol/cm^3]	The concentration of phenol of the TBR
$Cp\mathrm{h},L$	[mol/cm^3]	The concentration of phenol in liquid phase of the TBR
$Cp\mathrm{h},L(in)$	[ppm]	The initial phenol concentration of TBR
$Cp\mathrm{h},L(out)$	[ppm]	The outlet phenol concentration of TBR
$Cp\mathrm{h},L-S$	[mol/cm^3]	The concentration of phenol in the liquid-solid interface of the TBR
$Cw(x)$	[$kmol/m^3$]	The phenol concentration in the membrane wall in any point across the x-axis of the RO feed channel
Qf	[$kmol/m^3$]	The concentration of the feed
Qr	[kg/m^3]	The concentration of the retentate
$Db(x)$	[m^2/s]	The diffusivity parameter of feed in any point along the x-axis of the feed channel of the RO
Dei	[cm^2/s]	The effective diffusivity of the TBR
Dkn,i	[cm^2/s]	The Knudsen diffusivity of the TBR
D^{L}_{ph}	[cm^2/s]	The molecular diffusivity of phenol in the liquid phase of the TBR
D^{L}_{O2}	[cm^2/s]	The molecular diffusivity of oxygen in the liquid phase of the TBR
dp	[cm]	The diameter of catalyst particle of the TBR
dpe	[cm]	The equivalent particle diameter of the catalyst in the TBR
Dr	[cm]	The TBR reactor diameter
Dr^L	[cm^2/s]	The radial mass dispersion coefficient

dt	[cm]	The TBR tube diameter
EA	[J/mol K]	The activation energy of the TBR
eff_{erd}	[kWh/m^3]	The efficiency of the energy recovery device
$Fb(x)$	[m^3/s]	The feed flow rate in any point across the x-axis of the RO feed channel
$Fb(0)$	[m^3/s]	The inlet feed flow rate of the RO feed channel
$Fp(x)$	[m^3/s]	The permeate flow rate in any point across the x-axis of the RO permeate channel
$Fp(L)$	[m^3/s]	The total permeated flow rate of the RO
$HO2$	[Dimensionless]	The henry's law constant for the dissolved oxygen in TBR water
$Js(x)$	[kmol/m^2 s]	The phenol molar flux in any point across the x-axis of the RO feed channel
$Jw(x)$	[m/s]	The water flux in any point across the x-axis of the RO feed channel
$k(x)$	[m/s]	The mass transfer coefficient in any point across the x-axis of the RO feed channel
KGL	[cm/s]	The gas-to-liquid mass transfer coefficient of the TBR
$Khet$	[mol/cm^3]$^{1-n}$ s^{-1}	The reaction rate constant of the TBR process
KLS	[cm/s]	The liquid-to-solid mass transfer coefficient of the TBR
Kph	[cm^3/s]	The adsorption equilibrium constant of phenol of the TBR
K $_{L_{O2}}$	[cm^3/s]	Gas-liquid mass transfer coefficient of the TBR process
kgbw	[kg]	Body weight
L	[m]	The length of the RO membrane
LHSV	[h^{-1}]	The liquid hourly space velocity of the TBR
Lr	[cm]	The TBR bed length of reactor
n	[Dimensionless]	The order of phenol concentration in the TBR
m	[Dimensionless]	The order of oxygen partial pressure in the TBR
MWph :	[Dimensionless]	The molecular weight of phenol
$MWO2$	[Dimensionless]	The molecular weight of oxygen
P	[bar]	The partial pressure of oxygen of the TBR process
P_b	[atm]	The pressure of the bulk phenol in the feed
$Pb(0)$	[atm]	The inlet feed pressure of the RO feed channel
$Pb(x)$	[atm]	The feed pressure in any point across the x-axis of the RO feed channel
Pc	[psia]	The critical pressure of phenol in the TBR
Pp	[atm]	The permeate pressure in the RO permeate channel
Pf	[atm]	The pressure of the feed
Qf	[m^3/s]	The flowrate of the feed
Qp	[m^3/s]	The flowrate of the permeate stream
Qr	[m^3/s]	The flowrate of the retentate stream
R	[J/mol K]	Gas law constant (R = 0.082 $\frac{atm\ m^3}{°K\ kmol}$) , (8.314 $\frac{J}{mol\ K}$)
R101	[Dimensionless]	The name of RO stage on gPROMS
R102	[Dimensionless]	The name of RO stage on gPROMS
Rec	[Dimensionless]	The water recovery coefficient of the RO
rg	[cm]	The mean pore radius of the TBR
Rej_{RO}	[Dimensionless]	The phenol rejection coefficient of the RO
Rej_{TBR}	[Dimensionless]	The phenol rejection coefficient of TBR

rp	[cm]	The radius of the TBR catalyst particle
Rph	[mol/cm3cat s]	The rate disappearance of phenol per unit volume of catalyst in the TBR
Sg	[cm^2/g]	The specific surface area of the particles in the TBR
Sp	[cm^2]	The TBR total geometric surface area of catalyst
SR	[Dimensionless]	The phenol rejection
T	[°C]	The reaction temperature of the TBR
Tbr	[Dimensionless]	The TBR reduced boiling point temperature
Tc	[K]	The critical temperature of phenol in the TBR
tf	[mm]	The feed spacer thickness of the RO
Tr	[K]	The reduced temperature of the TBR
TRO	[°C]	The feed temperature of the RO
ug	[cm/s]	The TBR superficial gas velocity
ul	[cm/s]	The TBR superficial liquid velocity
$_{vc}L$	[cm^3/gmol]	The critical volume of liquid in the TBR
$_{vc}p$h	[cm^3/gmol]	The critical volume of phenol in the TBR
$Vcat$	[cm^3]	The volume of catalyst in the TBR
Vg	[cm^3/g]	The total pore volume in the TBR
vL	[cm^3/gmol]	The molar volume of liquid in the TBR
vO_2	[cm^3/gmol]	The molar volume of oxygen in the TBR
Vp	[cm^3/gmol]	The total geometric volume of catalyst particle in the TBR
W	[m]	The width of the RO membrane
WR	[%]	The phenol recovery
x	[m]	The length of RO membrane
Z	[cm]	The TBR catalyst bed length
Zc	[Dimensionless]	The critical compressibility factor of phenol
ZO_2	[Dimensionless]	The oxygen compressibility factor in the TBR process
ηLS	[Dimensionless]	The wetting efficiency of the TBR
η0	[Dimensionless]	The effectiveness factor of the TBR
εB	[Dimensionless]	The bed void fraction (bed porosity) of the TBR
$\varepsilon 1$	[Dimensionless]	The liquid phase fraction
ρcat	[g/cm^3]	The catalyst density of the TBR
ρph	[g/cm^3]	The density of phenol of the TBR
$\rho O2$	[g/cm^3]	The density of oxygen of the TBR
μph	[m Pa s]	The viscosity of phenol of the TBR
φ	[Dimensionless]	The Thiele modulus of the TBR
τ	[Dimensionless]	The tortuosity factor of the TBR

References

Abbas, A., 2005. Simulation and analysis of an industrial water desalination plant. *Chemical Engineering and Processing: Process Intensification*, 44(9), 999–1004.

Abdelkreem, M., 2013. Adsorption of Phenol from Industrial Wastewater Using Olive Mill Waste. *APCBEE Procedia*, 5, 349–357.

AlEisa, E., AlShayji, K., 2019. Analysis on Reclamation and Reuse of Wastewater in Kuwait. *Journal of Engineering Research - Kuwait University*, *7*(1).

Altaee, A. (2012). *Computational model for estimating reverse osmosis system design and performance: Part-one binary feed solution. Desalination, 291, 101–105.* doi:10.1016/j.desal.2012.01.028

Al-hotmani, O.M.A., Al-Obaidi, M.A.A., John, Y.M., Patel, R., Mujtaba, I.M., 2020. An Innovative Design of an Integrated MED-TVC and Reverse Osmosis System for Seawater Desalination: Process Explanation and Performance Evaluation. *Processes*, 8(5), 607.

Alhumoud, J.M. et al., 2010. Cost/Benefit Evaluation Of Sulaibiya Wastewater Treatment Plant In Kuwait. *International Business & Economics Research Journal (IBER)*, 9(2).

Al-Obaidi, M., Kara-Zaïtri, C., Mujtaba, I., 2017. Development of a mathematical model for apple juice compounds rejection in a spiral-wound reverse osmosis process. *Journal of Food Engineering*, 192, 111–121.

Al-Obaidi, M.A., Jarullah, A.T., Kara- Zaïtri, C., Mujtaba, I.M., 2018a. Simulation of hybrid trickle bed reactor–reverse osmosis process for the removal of phenol from wastewater. *Computers and Chemical Engineering*, 113, 264-273.

Al-Obaidi, M.A., Kara-Zaïtri, C., Mujtaba, I.M., 2018b. Optimal Reverse Osmosis Network Configuration for the Rejection of Dimethylphenol from Wastewater. *Journal of Environmental Engineering*, 144(1), 04017080.

Al-Obaidi, M., Kara-Zaïtri, C., Mujtaba, I., 2018c. Simulation and optimisation of spiral-wound reverse osmosis process for the removal of N -nitrosamine from wastewater. *Chemical Engineering Research and Design, 133*, 168-182. doi:10.1016/j.cherd.2018.03.012

Al-Obaidi, M., Kara-Zaïtri, C., Mujtaba, I., 2018d. Performance evaluation of multi-stage and multi-pass reverse osmosis networks for the removal of N-nitrosodimethylamine -D6 (NDMA) from wastewater using model-based techniques. *Journal of Environmental Chemical Engineering*, 6(4), 4797–4808.

Al-Obaidi, M., Kara-Zaïtri, C., Mujtaba, I.M., 2020. Wastewater Treatment by Reverse Osmosis Process.

Akashah, S. et al., 1987. Cost and economic analysis of Doha reverse osmosis plant (Kuwait). *Desalination*, 64, pp.65–82.

Anku, W. W., Mamo, M. A., & Govender, P. P. (2017). Phenolic compounds in water: Sources, reactivity, toxicity and treatment methods. *Phenolic Compounds - Natural Sources, Importance and Applications.* doi:10.5772/66927

Carina, S., Agata, A., Claus, H., 2017. Combined forward osmosis-reverse osmosis for the treatment of brewery wastewater.

Chakraborty, A., Roy, A., 2020. Water–energy nexus for estuarine systems with seasonal salinity variations: A thermodynamic feasibility analysis of reverse osmosis (RO)–pressure retarded osmosis (PRO) combinations. *Water Supply, 20*(6), 2415-2427. doi:10.2166/ws.2020.144

Duran-Llacer, I., Munizaga, J., Arumí, J. L., Ruybal, C., Aguayo, M., Sáez-Carrillo, K., Rojas, O., 2020. Lessons to Be Learned: Groundwater Depletion in Chile's Ligua and Petorca Watersheds through an Interdisciplinary Approach. *Water, 12*(9), 2446. doi:10.3390/w12092446

Dupont, R., 1982. Reverse Osmosis in the Treatment of Drinking Water.

Gami A., 2014. Phenol and its toxicity. *Journal of Environmental Microbiology and Toxicology*, 2(1).

Garud, R.M., Kore, S.V., Kore, V.S., Kulkarni, G.S., 2011. A Short Review on Process and Applications of Reverse Osmosis. *Universal Journal of Environmental Research and Technology*, 1(3).

gPROMS, 2004. Introductory User Guide. *Process Systems Enterprise Ltd.*

Gude, V. G., 2011. Energy consumption and recovery in reverse osmosis. *Desalination and Water Treatment, 36*(1-3), 239-260. doi:10.5004/dwt.2011.2534

Huang, X., Min, J.H., Lu, W., Jaktar, K., Yu, C., Jiang, S.C., 2015. Evaluation of methods for reverse osmosis membrane integrity monitoring for wastewater reuse. *Journal of Water Process Engineering*, 7, 161-168.

Mnif, A., Tabassi, D., Ben Sik Ali, M., & Hamrouni, B. (2015). Phenol removal from water by AG reverse Osmosis membrane. *Environmental Progress & Sustainable Energy*, *34*(4), 982-989.

Mohammed, A.E., Jarullah, A.T., Gheni, S.A., Mujtaba, I.M., 2016. Optimal design and operation of an industrial three phase reactor for the oxidation of phenol. *Computers and Chemical Engineering*, 94, 257-271.

Mohammadi, S., Kargari, A., Sanaeepur, H., Abbassian, K., Najafi, A., Mofarrah, E., 2015. Phenol removal from industrial wastewaters: a short review. *Desalination and Water Treatment*, 53(8), 2215-2234.

Schwinge, J., Neal, P.R., Wiley, D.E., Fletcher, D.F., Fane, A.G., 2004. Spiral wound modules and spacers: review and analysis. *Journal of membrane science*, 242(1-2), 129-153.

Spellman, F.R., 2020. Handbook of Water and Wastewater Treatment Plant Operations.

Tee, P.F. et al., 2016. Review on hybrid energy systems for wastewater treatment and bio-energy production. *Renewable and Sustainable Energy Reviews*, 54, pp.235–246.

Toth, A. J. (2020). *Modelling and Optimisation of Multi-Stage Flash Distillation and Reverse Osmosis for Desalination of Saline Process Wastewater Sources. Membranes, 10(10), 265.* doi:10.3390/membranes10100265

Villegas, L.G.C., Mashhadi, N., Chen, M., Mukherjee, D., Taylor, K.E., Biswas, N., 2016. A short review of techniques for phenol removal from wastewater. *Current Pollution Reports,* 2(3), 157-167.

Wu, C., Tu, X., 2016. Biological and fermentative conversion of syngas. *Handbook of Biofuels Production*, 335–357.

Appendix A

Table A.1. TBR model equations developed by (Mohammed et al., 2016).

Model Equation	Description	No.
$\frac{dCo_{2,G}}{dZ} = -(\frac{K_{GL}a_{GL}}{u_g})(\frac{Co_{2,G}}{Ho_2} - Co_{2,L})$	The equation used to find the oxygen concentration and mass transfer over the gas-liquid interface.	1
$\frac{dC_{ph,L}}{dZ} = -(\frac{\eta_{LS}K_{LS}a_{LS}}{u_l})(C_{ph,L} - C_{ph,L-S})$	The mass balance equation used to find the phenol concentration in the liquid phase.	2
$\frac{dCo_{2,G}}{dZ} = -\left(\frac{K_{GL}a_{GL}}{u_l}\right)\left(\frac{Co_{2,G}}{Ho_2} - Co_{2,L}\right) - (\frac{n_{L,S}K_{L,S}a_{L,S}}{u_l})(Co_{2,L} - Co_{2,L-S})$	The mass balance equation used to find the oxygen concentration in the liquid phase.	3
$K_{LS}a_{LS}(C_{ph,L} - C_{ph,L-s}) = \eta_0(1-\varepsilon_B)R_{ph}$	The chemical reaction of phenol.	4
$K_{LS}a_{LS}(C_{o2,L} - C_{o2,L-s}) = 7\eta_0(1-\varepsilon_B)R_{ph}$	The chemical reaction of oxygen.	5
$R_{ph} = \rho_{cat}K_{het}\frac{C_{ph}^n C_{O_2}^m}{(1+K_{ph}C_{ph,L})^2}$	The Langmuir–Hinshelwood kinetic equation used to find the phenol disappearance.	6
$K_{ph} = exp\,(-\frac{364.47}{T} - 2.3854)$	The equation used to find the adsorption equilibrium constant of phenol (K_{ph})	7
$K_{net} = A^0 exp\,(-\frac{EA}{RT})$	The equation used to find the reaction rate constant (K_{net})	8
$\frac{K_{O_2}^L a_L}{D_{O_2}^L} = 7(\frac{\rho_{ph}u_1}{\mu_{ph}})^{0.4}(\frac{\mu_{ph}}{\rho_{ph}D_{O_2}^L})^{0.5}$	The equation used to find the mass transfer coefficient of phenol in the gas-liquid interface.	9
$\frac{K_{ph}^s}{D_{ph}^L a_{LS}} = 1.8(\frac{\rho_{ph}u_1}{a_{LS}\mu_{ph}})^{0.5}(\frac{\mu_{ph}}{\rho_{ph}D_{ph}^L})^{1/3}$	The equation used to find the mass transfer coefficient of oxygen in the liquid-solid interface.	10
$\frac{K_{O_2}^s}{D_{O_2}^L a_{LS}} = 1.8(\frac{\rho_{ph}u_1}{a_{LS}\mu_{ph}})^{0.5}(\frac{\mu_{ph}}{\rho_{ph}D_{O_2}^L})^{1/3}$	The equation used to find the mass transfer coefficient of oxygen in the liquid-solid interface.	11
$D_{ph}^L = 8.93\times10^{-8}\frac{v_L^{0.267}T}{v_{ph}^{0.267}\mu_{ph}}$	The equation used to find the molecular diffusivity of phenol.	12
$D_{O_2}^L = 8.93\times10^{-8}\frac{v_L^{0.267}T}{v_{O_2}^{0.267}\mu_{ph}}$	The equation used to find the molecular diffusivity of oxygen.	13
$V_L = 0.285(Vc^L)^{1.048}$	The equation used to find molar volume of liquid.	14
$V_{ph} = 0.285(Vc^{ph})^{1.048}$	The equation used to find molar volumes of phenol.	15
$V_{O_2} = 0.285(Vc^{O_2})^{1.048}$	The equation used to find oxygen.	16
$H_{O_2} = (6088.8 - 871.2lnT - \frac{326284}{T})$	The equation used to find the Henry's constant for oxygen.	17
$\rho_{ph} = \frac{MW_{ph}P_c}{RT_cZ_c(1-T_r)^{\frac{2}{7}}}$	The equation used to find the density of phenol.	18
$T_r = \frac{T}{T_c}$	The equation used to find the reduced temperature of the reaction.	19
$\rho_{O_2} = \frac{PMW_{O_2}}{Z_{O_2}RT}$	The equation used to find the density of oxygen.	20
$\mu_{ph} = exp\left(ln(ax\mu_{ph,b}) \times \left(\frac{ln\,ln\,(\mu_{ph,b})}{ln\,ln\,(ax\mu_{ph,b})}\right)^{\emptyset}\right)$	The equation used to find the viscosity of phenol.	21

$\emptyset = \frac{1 - T_r}{1 - T_{br}}$	The equation used to find the volume fraction of molecules ($\emptyset$).	22
$T_{br} = \frac{T_b}{T_c}$	The equation used to find reduced boiling point temperatures.	23
$\eta_0 = \frac{3(\varphi coth\varphi - 1)}{\varphi^2}$	The equation used to find effectiveness factor of sphere particles.	24
$\varphi = \frac{V_p}{S_p}\sqrt{(\frac{n+1}{2})(\frac{K_{net} C_{ph}^{n-1} \rho_p}{D_{ei}})}$	The equation used to find the Thiel modulus (φ).	25
$\rho_p = \frac{\rho_{cat}}{1 - \varepsilon_B}$	The equation used to find the particle density (ρp).	26
$\varepsilon_B = 0.38 + 0.073\left(1 + \frac{(\frac{d_t}{d_{pe}} - 2)^2}{(\frac{d_t}{d_{pe}})^2}\right)$	The equation used to find the bed porosity (εB).	27
$V_p = \frac{4}{3}\pi(rp)^2$	The equation used to find the external volume of spherical particles.	28
$S_p = 4\pi(rp)^2$	The equation used to find the surface area (S_p) of spherical shape of particles.	29
$a_{L,S} = \frac{S_p(1 - \varepsilon_B)}{V_p}$	The equation used to find the surface area of particles per unit volume of the reactor bed.	30
$D_{ei} = \frac{\varepsilon_S}{\tau} \frac{1}{\frac{1}{D_{mo,i}} + \frac{1}{D_{kn,i}}}$	The equation used to find the effective diffusivity (D_{ei}).	31
$\varepsilon_S = \rho_P V_g$	The equation used to find the particle porosity of the catalyst (ε_S).	32
$D_{kn,i} = 9700\, r_g \sqrt{\frac{T}{MW_{ph}}}$	The equation used to find the Knudsen diffusivity ($D_{kn,i}$).	33
$r_g = 2\frac{V_g}{S_g}$	The equation used to find the mean pore radius (r_g).	34
$Rej_{TBR} = \frac{C_{ph,L(in)} - C_{ph,L(out)}}{C_{ph,L(in)}} \times 100$	The equation used to find the phenol rejection.	35

1

Appendix B

Table B.1. Single membrane RO model equations developed by (Al-Obaidi et al., 2018a)

Model Equation	Description	No.
$F_{b(x)} = \left\{F_{b(0)} - \left(W\theta x \triangle P_{b(0)}\right) + \left(W\theta b\frac{x^2}{2}F_{b(0)}\right) + \left(W\theta b(\frac{W\theta}{b})^{0.5}\left(\frac{x^2}{2}\right)(\triangle P_{b(x)} - \triangle P_{b(0)})\right)\right\}$	The equation used to find feed flowrate at any point about the x-axis.	1
$\theta = \frac{A_w B_s}{B_s + RT_{RO}A_w Cp_{(av)}}$	The equation used to calculate parameter in various equations.	2
$U_{b(x)} = \frac{F_{b(x)}}{t_f W}$	The equation used to find the feed velocity at any point about the x-axis.	3
$P_{b(x)} = \left\{P_{b(0)} - \left(bxF_{b(0)}\right) + \left(bW\theta\left(\frac{x^2}{2}\right)(\Delta P_{b(x)}\right) - \left[b^2W\theta\left(\frac{x^3}{6}\right)F_{b(0)}\right] - [\, b^2W\theta\left(\frac{W\theta}{b}\right)^{0.5}\left(\frac{x^3}{6}\right)(\Delta P_{b(x)} - \Delta P_{b(0)})\,]\right\}$	The equation used to find the feed pressure at any point about the x-axis.	4
$\Delta P_{b(x)} = \Delta P_{b(0)} - (b\ x\ F_{b(0)}) - \left[\left(\frac{W\theta}{b}\right)^{0.5} bx(\Delta P_{b(x)} - \Delta P_{b(0)})\right]$	The equation used to find the pressure differences of the feed channel and permeate channel at any point about the x-axis.	5
$\Delta P_{b(x)} = P_{b(0)} - P_p$	The equation used to find the pressure differences of the feed channel and permeate channel at x=0.	6
$J_{w(x)} = \theta\left\{\left[\Delta P_{b(0)} - (bxF_{b(0)})\right] - \left[\left(\frac{W\theta}{b}\right)^{0.5} bx(\Delta P_{b(x)} - \Delta P_{b(0)})\right]\right\}$	The equation used to find the water flux at point about the x-axis.	7
$J_{s(x)} = B_s(C_{w(x)} - Cp_{(av)})$	The equation used to find the solute flux at any point about the x-axis.	8
$\frac{C_{w(x)} - Cp_{(av)}}{C_{s(x)} - Cp_{(av)}} = exp\left(\frac{J_{w(x)}}{k_{(x)}}\right)$	The equation used to find the wall solute concentrate at any point about the x-axis.	9
$k_{(x)} = 1.177\left(\frac{U_{b(x)}D_{b(x)}^2}{t_f L}\right)^{0.3333}$	The equation used to find the mass transfer coefficient at any point about the x-axis.	10
$D_{b(x)} = 6.725E-6\ exp\left\{0.1546E-3\ C_{b(x)}(18.012) - \frac{2513}{T_{RO}+273.15}\right\}$	The equation used to find the diffusivity parameter at any point about the x-axis.	11
$\frac{C_{b(x)}}{t_f W}\frac{dF_{b(x)}}{dx} + \frac{F_{b(x)}}{t_f W}\frac{dC_{b(x)}}{dx} = \frac{d}{dx}\left[D_{b(x)}\frac{dC_{b(x)}}{dx}\right] - \frac{(J_{w(x)}Cp_{(x)})}{t_f} + \frac{J_{w(x)}C_{b(x)}}{t_f}$	The equation used to find the phenol feed concentration at any point about the x-axis.	12
$Cp_{(av)} = \frac{Cp_{(0)} + Cp_{(L)}}{2}$	The equation used to find the average permeate solute concentration.	13
$Cp_{(0)} = \frac{B_s\ C_{b(0)}\ e^{\frac{J_{w(0)}}{k(0)}}}{J_{w(0)}\ B_s\ e^{\frac{J_{w(0)}}{k(0)}}}$	The equation used to find the permeate solute concentration at x=0.	14
$Cp_{(L)} = \frac{B_s\ C_{b(L)}\ e^{\frac{J_{w(L)}}{k(L)}}}{J_{w(L)}\ B_s\ e^{\frac{J_{w(L)}}{k(L)}}}$	The equation used to find the permeate solute concentration at x=L.	15
$F_{p(X)} = F_{p(0)} + \left(Wx\theta\Delta P_{b(0)}\right) - \left[W\theta b\left(\frac{x^2}{2}\right)F_{b(0)}\right] - \left[W\theta b\left(\frac{x^2}{2}\right)\left(\frac{W\theta}{b}\right)^{0.5}(\Delta P_{b(x)} - \Delta P_{b(0)})\right]$	The equation used to find the permeated flowrate at pint about the x-axis.	16

$Rec_{(Total)} = \frac{F_{p(L)}}{F_{b(0)}} \times 100$	The equation used to find the total water recovery.	17
$Rej_{RO} = \frac{C_{b(0)} - Cp_{(av)}}{C_{b(0)}} \times 100$	The equation used to find the solute rejection.	18